Transport and entanglement for single photons in optical waveguide ladders

Junhua Dong, Qian Jiang, Qingmei Hu, Bingsuo Zou, and Yongyou Zhang*
Beijing Key Lab of Nanophotonics & Ultrafine Optoelectronic Systems and School of Physics, Beijing Institute of Technology, Beijing 100081, China

(Received 10 January 2019; published 22 July 2019)

Transfer and scattering matrix theories are derived for studying single-photon (SP) transport in optical waveguide ladders (OWLs). The OWLs consist of two one-dimensional waveguides connected by Jaynes-Cummings emitters (JCEs) and have two input and two output channels. The von Neumann entropy is introduced to describe the entanglement between the transmitted states from the two output channels. Two types of the OWLs are studied, i.e., the OWLs with two identical waveguides (i-OWLs) and those with two different waveguides (d-OWLs). When the OWLs contain only one JCE, the SP transport behavior in the i-OWLs is the same as that in the d-OWLs. When two JCEs are introduced, the quantum interference among the JCE-scattered waves can lead to the SP jumping with a 100% chance between the waveguides for the i-OWLs, while this is hard for the d-OWLs. As a result, the i-OWLs can serve as a SP router with respect to the d-OWLs. When the number of JCEs increases to a large value (e.g., 16), the transmission probabilities of the two output channels both tend to be 0.25 for the i-OWLs, but zero for d-OWLs. Correspondingly, the entanglements approximate a constant of 1 for the i-OWLs, but of zero for the d-OWLs. It shows that a large number of JCEs can suppress the influence of other system parameters including the SP frequency and JCE loss. Therefore, the i-OWLs with a large number of the JCEs show potential for a SP splitter and entanglement generator.

DOI: 10.1103/PhysRevA.100.013840

I. INTRODUCTION

One-dimensional (1D) waveguides [1–5] show many diversities in quantum informatics as they couple with quantum emitters, since such types of optical structures can tune the transport of photon states [6–10]. Quantum emitters, including quantum dots [11–13], two-level atoms [14–20], side optical cavities [21,22], and cavities with an atom [23–26] or Kerr medium [27] inside, are responsible for plenty of physical phenomena, for example, electromagnetically induced transparency [28–31], Fano resonance [32–34], polarization effects [35], slow light behavior [29,36], and multiphoton transmission [37,38]. Photons, as information carriers, fly in the 1D waveguide, which could be controlled by the quantum emitters coupled with the waveguides, behaving as a gate. Since the two ends of the waveguide are two natural ports for introducing and extracting information, the photonic architecture of the waveguide coupled with quantum emitters is a candidate for designing complex optical quantum devices. Some quantum devices based on this architecture have been proposed or implemented, such as frequency combs [3], photon memory [29], isolators [39], single-photon (SP) switching [40–43], transistors [44–46], band filters [47], SP frequency converters [48], and so on. The quantum interference between the guided photons and those emitted from the quantum emitters can result in a perfect reflection [49,50]. These works essentially focused on the architectures of a single 1D waveguide coupled with two-level systems or qubits on the SP level. These architectures could be achieved experimentally by superconducting circuits [51,52], neutral atoms [53–55], quantum dots in photonic crystals [56–59], and an optical cavity with an atom inside [60]. However, the architectures with many 1D waveguides are more interesting and powerful in practice because they can compose photonic quantum networks.

Quantum networks are profound subjects that can complete nonclassical tasks. One typical platform for quantum networks is based on cavity quantum electrodynamics [61], namely, photonic quantum networks that require suitable nodes and channels. Quantum emitters can serve as the quantum nodes and 1D waveguides are competent as the channels through which photons can transport over a long distance with almost negligible loss or decoherence [62,63]. Researchers have attempted to design quantum architectures based on a waveguide-emitter system to control the photon transport, such as SP level routers [64–69]. The quantum routers can redirect the incident photons to any of the output channels with an approximate unity probability. In the present work, we study the SP transport in the photonic quantum network shown in Fig. 1(a), i.e., an optical waveguide ladder (OWL) which consists of two 1D waveguides connected by Jaynes-Cummings emitters [(JCEs), being the cavity with one embedded two-level atom inside].

The SPs are incident from the two left ports of In 1 and In 2. The JCEs scatter them into the ports of In 1 and In 2 as reflection and into the two right ports of Out 1 and Out 2 as transmission. A similar structure also with two input ports and two output ports has been demonstrated in experiment for an all-optical SP router [70] (where the chiral coupling between the waveguide and one Λ-type atom was used), indicating that

*Author to whom correspondence should be addressed; yyzhang@bit.edu.cn

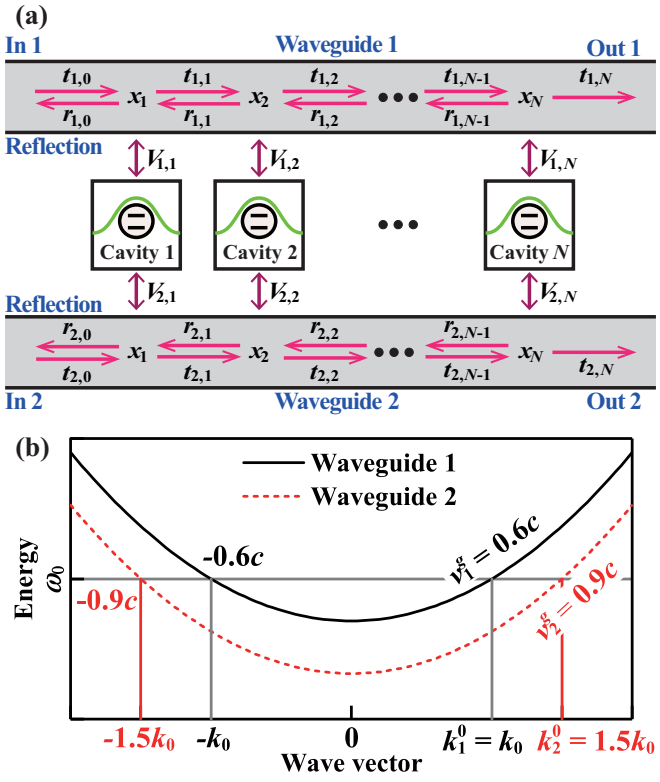

FIG. 1. (a) Schematic drawing of an optical waveguide ladder: two 1D waveguides are connected by N Jaynes-Cummings emitters (JCEs). The JCE is the optical cavity with an embedded two-level atom inside. The nth JCE located at x_n ($n = 1, 2, \ldots, N$) is coupled to waveguides 1 and 2 with strengths of $V_{1,n}$ and $V_{2,n}$, respectively. $t_{m,n}$ and $r_{m,n}$ ($m = 1, 2$) are the coefficients of the rightward and leftward moving photon in the mth waveguide between x_n and x_{n+1}. (b) Example of dispersions for two different waveguides. They have the group velocities of $\pm 0.6c$ and $\pm 0.9c$ at the energy of ω_0, corresponding to the wave vectors of $\pm k_0$ and $\pm 1.5k_0$, respectively, where c and k_0 are the vacuum light speed and unit of the wave vector.

the OWLs are achievable. As a rational conjecture, the reflection and transmission of the SPs in the OWL should present more potential with respect to the single-waveguide system, since one more waveguide is considered. For example, there is a correlation between the two transmitted states from the ports of Out 1 and Out 2 in the OWLs, while none in the single-waveguide system, since it has only one output port. The dispersions of the two waveguides can be the same as or different from each other, which brings us diversities also; see Fig. 1(b). For easy writing we denote the OWLs with two identical (different) waveguides as i-OWLs (d-OWLs). The number of the JCEs and group velocities of the waveguides show strong influence on the SP transport and entanglement of the two transmitted states. To describe them, the transfer and scattering matrix theories are built up and von Neumann entropy is introduced.

The rest of this work is organized as follows. In Sec. II, we first introduce the theoretical model for the OWL and then derive the transfer and scattering matrices for the SP transport. Subsequently, the SP transport properties are studied in Sec. III for the OWLs with identical and different waveguides. In Sec. IV, the entanglement between the two transmitted states is calculated and discussed. At last, a brief conclusion is summarized in Sec. V.

II. MODEL AND FORMULAS

A. Hamiltonian and wave functions

The OWL in Fig. 1(a) has two input ports, In 1 and In 2, and two output ports, Out 1 and Out 2. The JCEs connect the two waveguides at coordinates x_n. The Hamiltonian for the OWL is written as

$$H = H_W + H_{JC} + H_I, \tag{1}$$

where H_W, H_{JC}, and H_I describe the two waveguides, all isolated JCEs, and all interactions between the JCEs and waveguides, respectively. For convenience, the Planck constant is set to be $\hbar = 1$ hereafter.

To describe the SP transport properties in the OWLs, it is convenient to write H_W in the real space, which can be achieved by linearizing the waveguide dispersion [21]. Throughout this work, we denote the SP energy in the mth waveguide as $\varepsilon_m(k_m)$ with k_m being the corresponding wave vector. Around the concerned energy of ω_0, $\varepsilon_m(k_m)$ can be linearized as $\varepsilon_m(k_m) = (\omega_0 - v_m^g k_m^0) \pm v_m^g k_m$ for the right- and left-moving photons (v_m^g and k_m^0 are the group velocity and wave vector of the SP at the energy of ω_0, respectively); see Fig. 1(b). Accordingly, H_W has the form [21,43,44,71–74]

$$\begin{aligned} H_W = &\sum_{m=1}^{2} \int dx\, \hat{L}_m^\dagger(x) \left(\omega_0 - v_m^g k_m^0 + i v_m^g \frac{\partial}{\partial x} \right) \hat{L}_m(x) \\ &+ \sum_{m=1}^{2} \int dx\, \hat{R}_m^\dagger(x) \left(\omega_0 - v_m^g k_m^0 - i v_m^g \frac{\partial}{\partial x} \right) \hat{R}_m(x), \end{aligned} \tag{2}$$

where $\hat{L}_m^\dagger(x)$ and $\hat{L}_m(x)$ [$\hat{R}_m^\dagger(x)$ and $\hat{R}_m(x)$] are the creation and annihilation field operators for the left-moving (right-moving) photons at coordinate x in the mth waveguide.

For the Hamiltonian of the JCEs, the rotating wave approximation is often used to maintain the conservation law of particle number, namely, H_{JC} is written as [4,5,21,43]

$$\begin{aligned} H_{JC} = \sum_{n=1}^{N} \big[&\tilde{\omega}_n^c \hat{c}_n^\dagger \hat{c}_n + \tilde{\omega}_n^e \hat{e}_n^\dagger \hat{e}_n \\ &+ \omega^g \hat{g}_n^\dagger \hat{g}_n + \Omega_n (\hat{c}_n^\dagger \hat{\sigma}_n^- + \text{H.c.}) \big], \end{aligned} \tag{3}$$

where $\hat{c}_n^\dagger$ and $\hat{c}_n$ are the creation and annihilation operators of the nth cavity with the eigenfrequency of $\tilde{\omega}_n^c$. $\hat{e}_n^\dagger$ and $\hat{e}_n$ ($\hat{g}_n^\dagger$ and $\hat{g}_n$) are the creation and annihilation operators of the excited (ground) state with the energy of $\tilde{\omega}_n^e$ (ω^g) for the nth two-level atom. $\hat{\sigma}_n^+ = \hat{e}_n^\dagger \hat{g}_n$ ($\hat{\sigma}_n^- = \hat{g}_n^\dagger \hat{e}_n$) gives the atomic raising (lowering) ladder operator. The Rabi energy Ω_n describes the coupling between the atom and cavity. Besides, the nonzero imaginary parts of $\tilde{\omega}_n^c$ and $\tilde{\omega}_n^e$ give the non-Hermitian dissipative processes in the system, accounting for the leakage of photons into those nonwaveguide modes.

For the interaction between the JCEs and waveguides, the following δ-type coupling Hamiltonian is adopted

[5,43,71–73]:

$$H_I = \sum_{m=1}^{2}\sum_{n=1}^{N}\int dx\, V_{m,n}\delta(x-x_n)\{\hat{c}_n^\dagger[\hat{R}_m(x)+\hat{L}_m(x)]+\text{H.c.}\}, \tag{4}$$

where $V_{m,n}$ describes the coupling strength between the mth waveguide and nth cavity; see Fig. 1(a). This type of Hamiltonian has been proved to be effective as the frequency width of the incident pulsed wave is much smaller than the SP frequency. Under this condition, one can take the coupling strength between the JCEs and waveguides to be independent of the photon frequency [45], which corresponds to the Markovian approximation [75]. In addition, we assume that the distance between the two waveguides is much larger than the system characteristic length, so that the direct coupling between them can be neglected. This assumption is realizable in experiments [76,77], as long as the distance between the waveguides is about ten times of the system characteristic length.

For the single particle excitation, the eigenstate of H takes the form [5,71–73]

$$|\Phi\rangle = \left\{\sum_{m=1}^{2}\int dx[\mathcal{R}_m(x)\hat{R}_m^\dagger(x)+\mathcal{L}_m(x)\hat{L}_m^\dagger(x)] + \sum_{n=1}^{N}(\mathcal{C}_n\hat{c}_n^\dagger+\mathcal{A}_n\hat{\sigma}_n^+)\right\}|\varnothing\rangle, \tag{5}$$

where $|\varnothing\rangle$ is the vacuum state, i.e., no photon in any waveguide or any cavity, and all atoms are in the ground state. $\mathcal{C}_n$ ($\mathcal{A}_n$) represents the excitation amplitude of the nth cavity (atom). $\mathcal{R}_m(x)$ [$\mathcal{L}_m(x)$] is the wave function of the photon rightward (leftward) moving in the mth waveguide. For the architecture in Fig. 1(a), they have the following forms [10,44]:

$$\mathcal{R}_m(x) = e^{ik_m x}\Big[t_{m,0}\theta(x_1-x)+t_{m,N}\theta(x-x_N) + \sum_{n=1}^{N-1}t_{m,n}\theta(x-x_n)\theta(x_{n+1}-x)\Big], \tag{6}$$

$$\mathcal{L}_m(x) = e^{-ik_m x}\left[r_{m,0}\theta(x_1-x)+\sum_{n=1}^{N-1}r_{m,n}\theta(x-x_n)\theta(x_{n+1}-x)\right], \tag{7}$$

where $\theta(x)$ is the unit step function. $t_{m,n}$ and $r_{m,n}$ determine the SP wave functions and are denoted in Fig. 1(a) for clarity.

B. Transfer matrix theory

The SP transmission probability can be calculated by the transfer matrix, $\boldsymbol{M}_n$, connecting the coefficient vector $\boldsymbol{F}_n$ and $\boldsymbol{F}_{n-1}$, i.e.,

$$\boldsymbol{F}_n = \boldsymbol{M}_n\boldsymbol{F}_{n-1}, \tag{8}$$

where $\boldsymbol{F}_n$ is defined as

$$\boldsymbol{F}_n = \begin{pmatrix}\boldsymbol{t}_n\\ \boldsymbol{r}_n\end{pmatrix}, \tag{9}$$

with $\boldsymbol{t}_n = (t_{1,n}, t_{2,n})^T$ and $\boldsymbol{r}_n = (r_{1,n}, r_{2,n})^T$ (T gives the transpose of the vector). Substituting Eqs. (1) and (5) into the steady Schrödinger equation,

$$H|\Phi\rangle = \varepsilon|\Phi\rangle, \tag{10}$$

one can find $\boldsymbol{M}_n$ after some algebra derivations as follows:

$$\boldsymbol{M}_n = \boldsymbol{G}^{-1}\boldsymbol{Q}_n^*\begin{pmatrix}\boldsymbol{I}-i\boldsymbol{Y}_n & -i\boldsymbol{Y}_n\\ i\boldsymbol{Y}_n & \boldsymbol{I}+i\boldsymbol{Y}_n\end{pmatrix}\boldsymbol{Q}_n\boldsymbol{G}. \tag{11}$$

The detailed derivation for $\boldsymbol{M}_n$ is given in Appendix A. Here, $\boldsymbol{I}$ and $\boldsymbol{Y}_n$ are 2×2 matrices, namely,

$$\boldsymbol{I} = \begin{pmatrix}1 & 0\\ 0 & 1\end{pmatrix}, \quad \boldsymbol{Y}_n = \frac{1}{\zeta_n}\begin{pmatrix}J_{1,n} & \sqrt{J_{1,n}J_{2,n}}\\ \sqrt{J_{1,n}J_{2,n}} & J_{2,n}\end{pmatrix}, \tag{12}$$

where $\zeta_n = \varepsilon - \tilde{\omega}_n^c - \frac{\Omega_n^2}{\varepsilon-\tilde{\omega}_n^a}$ and $J_{m,n} = V_{m,n}^2/v_m^g$. The 4×4 diagonal matrices of $\boldsymbol{G}$ and $\boldsymbol{Q}_n$ are given by

$$\boldsymbol{G} = \text{diag}\big(\sqrt{v_1^g}, \sqrt{v_2^g}, \sqrt{v_1^g}, \sqrt{v_2^g}\big), \tag{13}$$

$$\boldsymbol{Q}_n = \text{diag}(e^{ik_1x_n}, e^{ik_2x_n}, e^{-ik_1x_n}, e^{-ik_2x_n}). \tag{14}$$

Here, diag$(\cdots)$ represents the diagonal matrix.

With $\boldsymbol{M}_n$ the total transfer matrix of $\boldsymbol{M}$ can be written as

$$\boldsymbol{M} = \boldsymbol{M}_N\boldsymbol{M}_{N-1}\cdots\boldsymbol{M}_1, \tag{15}$$

which determines the system transmission and reflection coefficients. According to Eq. (9), it is convenient to divide $\boldsymbol{M}_n$ and $\boldsymbol{M}$ into four 2×2 matrices, i.e.,

$$\boldsymbol{M}_n = \begin{pmatrix}\boldsymbol{M}_n^{tt} & \boldsymbol{M}_n^{tr}\\ \boldsymbol{M}_n^{rt} & \boldsymbol{M}_n^{rr}\end{pmatrix}, \quad \boldsymbol{M} = \begin{pmatrix}\boldsymbol{M}^{tt} & \boldsymbol{M}^{tr}\\ \boldsymbol{M}^{rt} & \boldsymbol{M}^{rr}\end{pmatrix}. \tag{16}$$

Finally, the reflection and transmission coefficients of $\boldsymbol{r}_0$ and $\boldsymbol{t}_N$ can be found as

$$\boldsymbol{r}_0 = -\big(\boldsymbol{M}^{rr}\big)^{-1}\boldsymbol{M}^{rt}\boldsymbol{t}_0, \tag{17}$$

$$\boldsymbol{t}_N = [\boldsymbol{M}^{tt}-\boldsymbol{M}^{tr}(\boldsymbol{M}^{rr})^{-1}\boldsymbol{M}^{rt}]\boldsymbol{t}_0. \tag{18}$$

Here, $\boldsymbol{t}_0$ represents the incident coefficient; see Fig. 1(a). It takes two possible values of $(1,\ 0)^T$ and $(0,\ 1)^T$, representing the incidence from the ports of In 1 and In 2, respectively. If we introduce $t_{mm'}$ ($r_{mm'}$) to denote the transmission (reflection) coefficient from port of In m' to that of Out m (In m), the corresponding transmission and reflection probabilities have the following expressions:

$$T_{mm'} = \frac{v_m^g}{v_{m'}^g}|t_{mm'}|^2, \quad R_{mm'} = \frac{v_m^g}{v_{m'}^g}|r_{mm'}|^2. \tag{19}$$

They depend on the group velocities when $v_1^g \neq v_2^g$ and have four components. When the two waveguides are the same as each other (implying $v_1^g = v_2^g$), they are just the absolute square of the coefficients, which is similar to the SP transport in the structure with only one waveguide [21].

C. Scattering matrix theory

Equation (12) indicates that the transfer matrix elements are very large as $\zeta_n \sim 0$, resulting in that the transfer matrix method may fail for the large N (number of the JCEs). This

problem can be overcome by the scattering matrix theory being more stable than the transfer matrix.

The scattering matrix of $\boldsymbol{S}_n$ is defined to connect the vectors $(\boldsymbol{t}_0, \boldsymbol{r}_n)^T$ and $(\boldsymbol{t}_n, \boldsymbol{r}_0)^T$,

$$\begin{pmatrix} \boldsymbol{t}_n \\ \boldsymbol{r}_0 \end{pmatrix} = \boldsymbol{S}_n \begin{pmatrix} \boldsymbol{t}_0 \\ \boldsymbol{r}_n \end{pmatrix} = \begin{pmatrix} \boldsymbol{S}_n^{tt} & \boldsymbol{S}_n^{tr} \\ \boldsymbol{S}_n^{rt} & \boldsymbol{S}_n^{rr} \end{pmatrix} \begin{pmatrix} \boldsymbol{t}_0 \\ \boldsymbol{r}_n \end{pmatrix}. \tag{20}$$

These connected coefficients, respectively, describe the incident and scattered waves with respect to the former n JCEs in the OWL; see Fig. 1(a). The total scattering matrix of $\boldsymbol{S}_N$ connects the incident and scattered waves of the OWL, i.e., $(\boldsymbol{t}_0, \boldsymbol{r}_N)^T$ and $(\boldsymbol{t}_N, \boldsymbol{r}_0)^T$, and can be found by the following iteration scheme:

$$\begin{aligned}
\boldsymbol{S}_n^{tt} &= \left(\boldsymbol{W}_n^{tt} - \boldsymbol{S}_{n-1}^{tr}\boldsymbol{W}_n^{rt}\right)^{-1}\boldsymbol{S}_{n-1}^{tt}, \\
\boldsymbol{S}_n^{tr} &= \left(\boldsymbol{W}_n^{tt} - \boldsymbol{S}_{n-1}^{tr}\boldsymbol{W}_n^{rt}\right)^{-1}\left(\boldsymbol{S}_{n-1}^{tr}\boldsymbol{W}_n^{rr} - \boldsymbol{W}_n^{tr}\right), \\
\boldsymbol{S}_n^{rt} &= \boldsymbol{S}_{n-1}^{rt} + \boldsymbol{S}_{n-1}^{rr}\boldsymbol{W}_n^{rt}\left(\boldsymbol{W}_n^{tt} - \boldsymbol{S}_{n-1}^{tr}\boldsymbol{W}_n^{rt}\right)^{-1}\boldsymbol{S}_{n-1}^{tt}, \\
\boldsymbol{S}_n^{rr} &= \boldsymbol{S}_{n-1}^{rr}\left[\boldsymbol{W}_n^{rt}\left(\boldsymbol{W}_n^{tt} - \boldsymbol{S}_{n-1}^{tr}\boldsymbol{W}_n^{rt}\right)^{-1}\left(\boldsymbol{S}_{n-1}^{tr}\boldsymbol{W}_n^{rr} - \boldsymbol{W}_n^{tr}\right) + \boldsymbol{W}_n^{rr}\right],
\end{aligned} \tag{21}$$

where $\boldsymbol{W}_n$ is the inverse of $\boldsymbol{M}_n$, i.e.,

$$\boldsymbol{W}_n = \boldsymbol{M}_n^{-1} = \begin{pmatrix} \boldsymbol{W}_n^{tt} & \boldsymbol{W}_n^{tr} \\ \boldsymbol{W}_n^{rt} & \boldsymbol{W}_n^{rr} \end{pmatrix}. \tag{22}$$

The detailed derivation for the iteration scheme of the scattering matrices is shown in Appendix B. When N is very large, the scattering matrix $\boldsymbol{S}_N$ should be used to calculate the transmission and reflection probabilities.

In numerical calculation, we take ω_0 and k_0 as the units of the energy and wave vector, and the corresponding length and velocity units are $\lambda_0 = 2\pi/k_0$ and vacuum light speed of c. All JCEs have the same parameters, that is, $\tilde{\omega}_n^c = \omega_c - i\gamma_c$, $\tilde{\omega}_n^a = \omega_a - i\gamma_a$, $\Omega_n = \Omega$, and $J_{mn} = J_m$. ω_c and γ_c (ω_a and γ_a) measure the cavity (two-level atom) eigenfrequency and loss, respectively. Other assumptions for the system parameters are as follows: $\omega_c = \omega_a = \omega_0$, $\Omega = 0.02\omega_0$, and $J_1 = J_2 = 0.005\omega_0$; for the i-OWLs $v_1^g = v_2^g = 0.6c$ and $k_1^0 = k_2^0 = k_0$, while for the d-OWLs $v_1^g = 0.6c$, $v_2^g = 0.9c$, $k_1^0 = k_0$, and $k_2^0 = 1.5k_0$ as an example; see Fig. 1(b). These values of the parameters are consistent with those used in the theoretical works [6,21,43,71,72] and experiments [60,70].

III. TRANSMISSION AND REFLECTION

This section is divided into two subsections: (A) i-OWLs and (B) d-OWLs. For the i-OWLs and d-OWLs the SP transport properties are calculated and compared with each other in detail.

A. i-OWLs

Figure 2 shows the SP transmission and reflection spectra for the i-OWLs with one JCE ($N = 1$). T_{11} and T_{22} have two dips at the two eigenfrequencies of the JCE (i.e., $0.98\omega_0$ and $1.02\omega_0$), while T_{21}, T_{12} and all $R_{mm'}$ present two peaks. Their

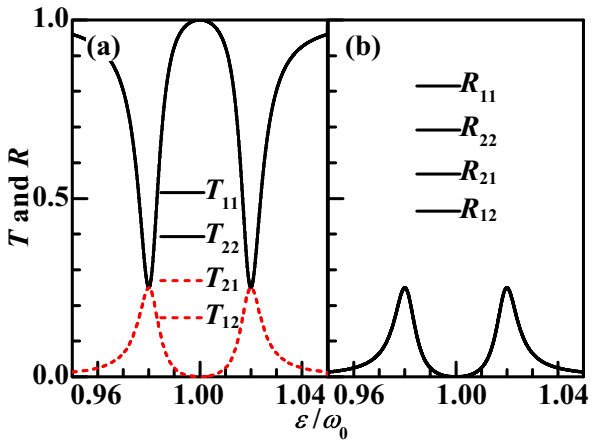

FIG. 2. SP transmission and reflection spectra for the i-OWLs with one JCE ($N = 1$). Parameters: $\omega_c = \omega_a = \omega_0$, $\Omega = 0.02\omega_0$, $J_1 = J_2 = 0.005\omega_0$, $k_1^0 = k_2^0 = k_0$, $v_1^g = v_2^g = 0.6c$, and $\gamma_a = \gamma_c = 0$.

expressions can be written as

$$T_{mm} = \left|\frac{1 + i\mathcal{J}_{\bar{m}}}{1 + i(\mathcal{J}_1 + \mathcal{J}_2)}\right|^2, \tag{23a}$$

$$R_{mm} = \left|\frac{-i\mathcal{J}_m}{1 + i(\mathcal{J}_1 + \mathcal{J}_2)}\right|^2, \tag{23b}$$

$$T_{m\bar{m}} = R_{m\bar{m}} = \left|\frac{-i\sqrt{\mathcal{J}_1\mathcal{J}_2}}{1 + i(\mathcal{J}_1 + \mathcal{J}_2)}\right|^2, \tag{23c}$$

where

$$\mathcal{J}_m = \frac{J_m}{\varepsilon - \omega_c + i\gamma_c - \frac{\Omega^2}{\varepsilon - \omega_a + i\gamma_a}}, \tag{24}$$

and $\bar{m} = 1$ and 2 when $m = 2$ and 1, respectively. Since $J_1 = J_2$, $\omega_c = \omega_a = \omega_0$, and $\gamma_c = \gamma_a = 0$ are adopted, the above expressions give $T_{11} = T_{22} = 1$ and zero for all other probabilities when $\varepsilon = \omega_0$; see Fig. 2. In this case, there is no SP jump between two waveguides. On the contrary, all transmission and reflection probabilities are equal to 0.25 for $\varepsilon = 0.98\omega_0$ and $1.02\omega_0$, showing a definite SP jumping. Combining these two situations, the i-OWLs could be used to adjust the SP probability distribution among the four ports.

The SP transport properties of the i-OWLs with one JCE can be compared with those of the single-waveguide structure coupled with one JCE (denoted as SWS) [21]. Let's first recall the expressions of the transmission and reflection probabilities of the SWS,

$$T = \left|\frac{\varepsilon - \omega_c + i\gamma_c - \frac{\Omega^2}{\varepsilon - \omega_a + i\gamma_a}}{\varepsilon - \omega_c + i\gamma_c - \frac{\Omega^2}{\varepsilon - \omega_a + i\gamma_a} + iJ}\right|^2, \tag{25a}$$

$$R = \left|\frac{-iJ}{\varepsilon - \omega_c + i\gamma_c - \frac{\Omega^2}{\varepsilon - \omega_a + i\gamma_a} + iJ}\right|^2, \tag{25b}$$

where J measures the coupling strength between the JCE and waveguide. Equations (25a) and (25b) are the same as Eqs. (23a) and (23b), respectively, under the mapping of $J \Leftrightarrow J_m$ and $\gamma_c \Leftrightarrow \gamma_c + J_{\bar{m}}$. Therefore, the influence of the second waveguide on the SP transport in the first one is just to

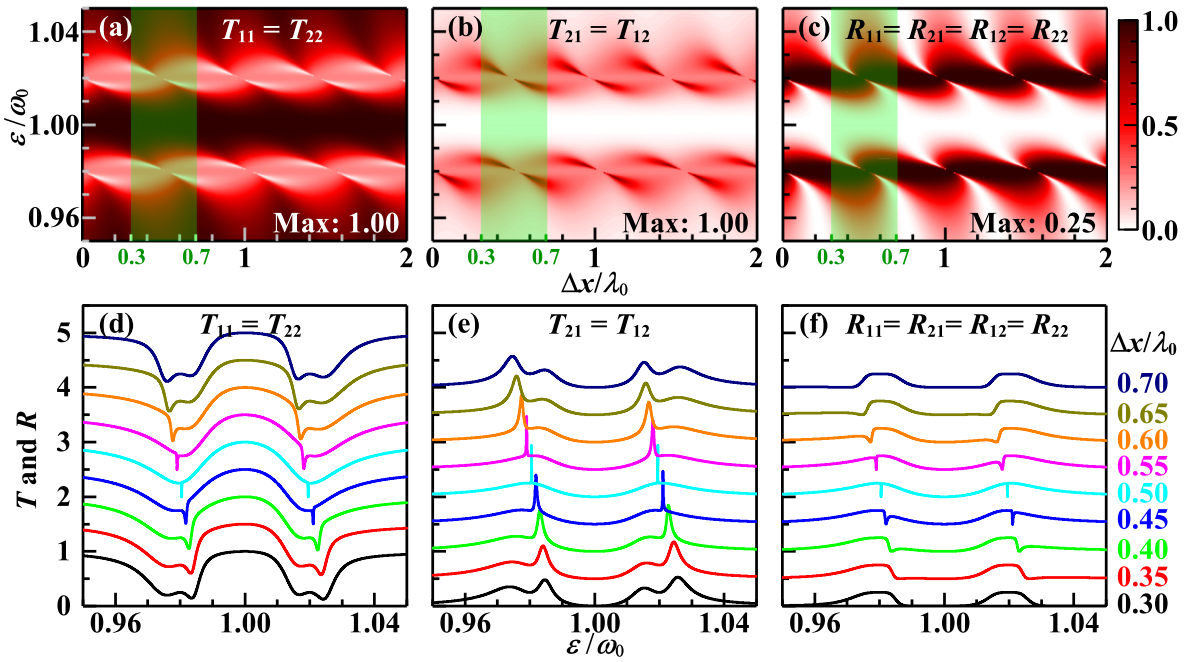

FIG. 3. (a)–(c) Contour maps of the transmission and reflection spectra for the i-OWLs with two JCEs ($N = 2$), as functions of the photon energy, ε, and distance between the two JCEs, Δx. Their values are normalized to their maxima denoted by "Max". (d)–(f) Transmission and reflection spectra for $\Delta x \in [0.3\lambda_0,\ 0.7\lambda_0]$ with a step of $0.05\lambda_0$, located in the light green region in (a)–(c), respectively. For easy observation, lines are offset from the bottom with a step of 0.5. Parameters: $\omega_c = \omega_a = \omega_0$, $\Omega = 0.02\omega_0$, $J_1 = J_2 = 0.005\omega_0$, $k_1^0 = k_2^0 = k_0$, $v_1^g = v_2^g = 0.6c$, and $\gamma_a = \gamma_c = 0$.

increase the cavity loss. In other words, the SWS with cavity loss can be mapped to the i-OWLs without cavity loss for the SP transport, implying that the i-OWLs are more general than the SWS.

From Eq. (23c) it is found that $T_{21} = T_{12}$ and neither of them could reach 1. When $J_1 = J_2$ is adopted in Fig. 2, we have $T_{11} = T_{22}$ and $T_{21} = T_{12} = R_{11} = R_{22} = R_{12} = R_{21}$. They tell that the SP jumping with a 100% chance between two waveguides cannot take place for the i-OWLs with one JCE, see Fig. 2, while the i-OWLs with two JCEs ($N = 2$) can; see Fig. 3, where the distance between the two JCEs is denoted as Δx. When more than one JCEs are introduced, these JCEs can induce the quantum interference among the scattered SP waves [74]. The quantum interference caused by the two JCEs has been studied for the single-waveguide model [73]. For the present two-waveguide model, i.e., the i-OWLs with two JCEs, the system transmission and reflection can be expressed as

$$T_{mm} = \left| \frac{1 + \mathcal{J}_{\bar{m}}[i2 + (\mathcal{J}_1 + \mathcal{J}_2)(e^{i2k\Delta x} - 1)]}{1 + i2(\mathcal{J}_1 + \mathcal{J}_2) + (\mathcal{J}_1 + \mathcal{J}_2)^2(e^{i2k\Delta x} - 1)} \right|^2, \quad (26a)$$

$$R_{mm} = \left| \frac{\mathcal{J}_m[(\mathcal{J}_1 + \mathcal{J}_2)(e^{i2k\Delta x} - 1) + i(e^{i2k\Delta x} + 1)]}{1 + i2(\mathcal{J}_1 + \mathcal{J}_2) + (\mathcal{J}_1 + \mathcal{J}_2)^2(e^{i2k\Delta x} - 1)} \right|^2, \quad (26b)$$

$$T_{m\bar{m}} = \left| \frac{\sqrt{\mathcal{J}_1\mathcal{J}_2}[i2 + (\mathcal{J}_1 + \mathcal{J}_2)(e^{i2k\Delta x} - 1)]}{1 + i2(\mathcal{J}_1 + \mathcal{J}_2) + (\mathcal{J}_1 + \mathcal{J}_2)^2(e^{i2k\Delta x} - 1)} \right|^2, \quad (26c)$$

$$R_{\bar{m}m} = \frac{\mathcal{J}_{\bar{m}}}{\mathcal{J}_m} R_{mm}, \quad (26d)$$

where the two waveguides in the i-OWLs have the same photon wave vector, k. The 100% chance of the SP jumping between two waveguides requires $T_{mm} = 0$, giving the condition of $1 + \mathcal{J}_{\bar{m}}[i2 + (\mathcal{J}_1 + \mathcal{J}_2)(e^{i2k\Delta x} - 1)] = 0$. When $\Delta x = 0$ it becomes $\mathcal{J}_{\bar{m}} = -i/2$, which is hardly satisfied; see Eq. (24). However, when $\Delta x \neq 0$ the condition becomes much easier to meet. For example, Fig. 3(b) shows that $T_{m\bar{m}}$ can reach 1 for some values of Δx. Since $J_1 = J_2$ is adopted in Fig. 3, it holds $T_{11} = T_{22}$, $T_{21} = T_{12}$, and $R_{11} = R_{21} = R_{12} = R_{22}$, which can be derived out from Eq. (26). To demonstrate the SP jumping between two waveguides, the transmission and reflection spectra are plotted in Figs. 3(d)–3(f), corresponding to Figs. 3(a)–3(c), respectively. For $\Delta x \sim 0.5\lambda_0$, $T_{m\bar{m}}$ has two sharp peaks up to 1 and, simultaneously, T_{mm} and $R_{mm'}$ have two sharp dips down to zero. These peaks and dips are broadened and no longer reach 1 and zero, respectively, when Δx is away from $0.5\lambda_0$. The quantum interference caused by the two JCEs is responsible for the SP jumping with a 100% chance between two waveguides. Different from this mechanism, the chiral coupling between the quantum emitters and waveguides was also proposed to achieve the SP jumping from one waveguide into another [68], which associates with the so-called spin-orbit interaction of light [78].

On the other hand, the quantum interference accounts for the periodical variation of the transmission and reflection probabilities with Δx; see Figs. 3(a)–3(c). Similar results have been shown for the single waveguide coupled with two JCEs in Ref. [73]. The period equals $\frac{2\pi}{2k} \sim 0.5\lambda_0$ for $k \sim k_0$. As a result, there are lots of values for Δx to achieve the SP jumping with a 100% chance between two waveguides. But for a certain Δx only two peaks in the spectra (near the two

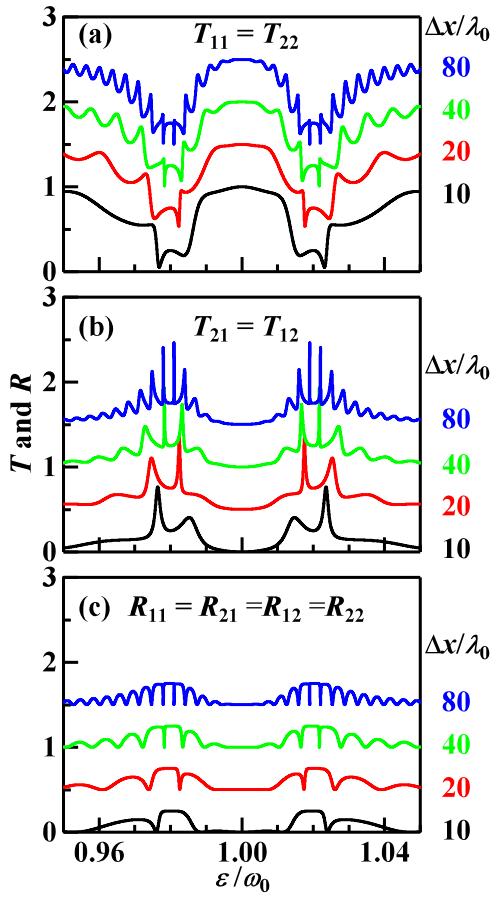

FIG. 4. Transmission and reflection spectra for the i-OWLs with two JCEs ($N = 2$) under four large values of Δx. Lines are offset from the bottom with a step of 0.5. Other parameters are the same as those for Fig. 3.

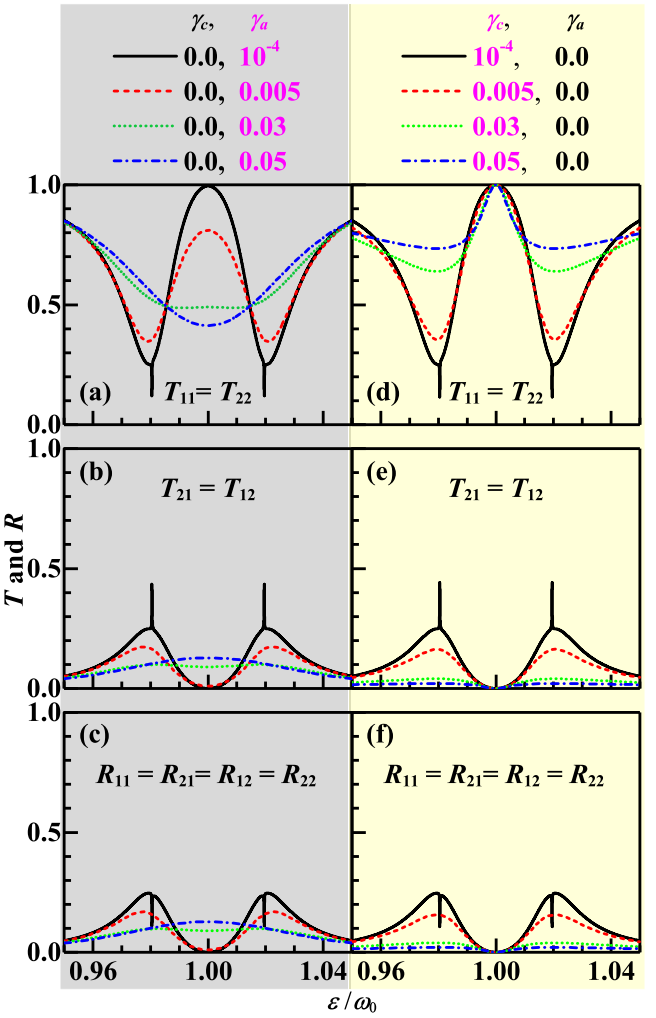

FIG. 5. Transmission and reflection spectra for the i-OWLs with two JCEs ($N = 2$) under four values of atom (left column) and cavity (right) losses. In calculation, $\Delta x = 0.5\lambda_0$ and other parameters are the same as those for Fig. 3.

JCE eigenfrequencies) meet such SP jumping; see Figs. 3(d)–3(f). Since the 100% chance of the SP jumping originates from the quantum interference caused by the two JCEs, we can further increase Δx to induce more resonant peaks in the transmission and reflection spectra; see Fig. 4. The distance of $\Delta\varepsilon$ between the two neighbor peaks is inverse proportional to Δx, i.e., $\Delta\varepsilon \sim v_g \frac{2\pi}{\Delta x}$, and thus the peak number increases for increasing Δx. The spectra of T_{21} and T_{12} near the two eigenfrequencies of the JCEs (i.e., $0.98\omega_0$ and $1.02\omega_0$) split into several peaks with values approaching 1; see Fig. 4(b). On the other hand, the SPs prefer to transport in identical waveguides when the frequency is away from these two eigenfrequencies, that is, T_{11} and T_{22} approach 1; see Figs. 3 and 4. Accordingly, researchers could design the output channel for the SPs in the i-OWLs.

Different from the i-OWLs with one JCE, the influence of the second waveguide in the i-OWLs with two JCEs cannot be mapped to the cavity loss in the SWS (also with two JCEs), owing to the quantum interference. Figure 5 shows the influence of the JCE loss (i.e., the losses of the atom and cavity) on the transmission and reflection spectra. Apparent sharp peaks for T_{21} and T_{12} can be found when γ_a and γ_c are both small, see Figs. 5(b) and 5(e), while they disappear as γ_a and γ_c increase. Since large γ_a and γ_c can depress the quantum interference caused by the two JCEs, they can also break down the 100% chance of the SP jumping between the two waveguides.

For the JCE works like a cavity when $\gamma_a > \Omega$ [see Eq. (24)], the spectra of T_{mm} gradually transform from the line shape with two dips to that with one as γ_a increases [see Fig. 5(a)]. On the contrary, for small γ_a the value of $T_{mm}|_{\varepsilon=\omega_0} \sim 1$ is almost independent of γ_c, see Eq. (26a), and thus the line shape of T_{mm} always maintains two dips when γ_c increases, even when $\gamma_c > \Omega$; see Fig. 5(d). The cavity and atom losses present different effects on the transmission and reflection spectra, but they both decrease the sharpness of the spectra. The losses of γ_a and γ_c should be less than one-tenth of the Rabi coupling between the atom and cavity for the SP jumping with a high chance between two waveguides. This efficient SP jumping can be realized by adjusting the distance between the two JCEs. We draw the conclusion that the quantum interference caused by the two JCEs can make the SP jumping from one waveguide to another efficiently, which makes the i-OWLs possible to serve as a SP router.

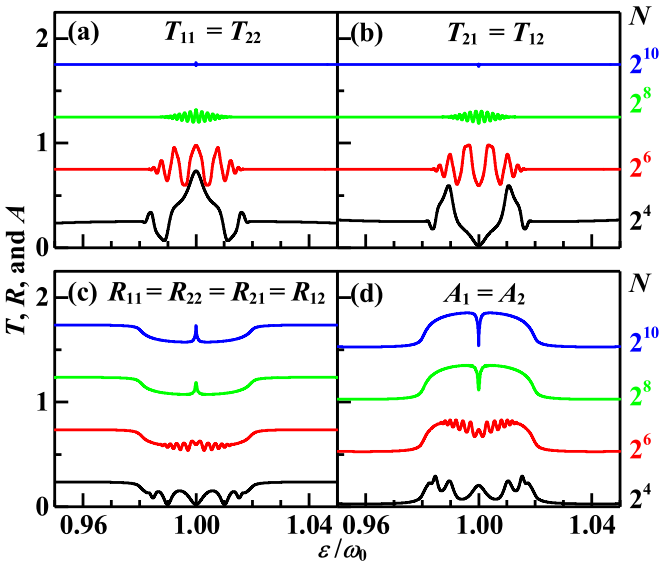

FIG. 6. Transmission, reflection, and absorption spectra for the i-OWLs with N JCEs. All JCEs are uniformly spaced and the nearest-neighbor distance is $\Delta x = 0.5\lambda_0$. Lines are offset from the bottom with a step of 0.5. In calculation, $\gamma_a = \gamma_c = 0.001\omega_0$ and other parameters are the same as those for Fig. 3.

Figures 2 to 5 show that the SP transmission and reflection depend on the SP frequency strongly. According to Eqs. (11), (12), and (15), this strong dependence may be avoided by considering more JCEs in the i-OWLs, because multiplication of many ζ_n [see Eq. (12)] in Eq. (15) could depress the influence of other system parameters; see Fig. 6, where four values of N are considered. For $N = 2^4$, there are several oscillations for T_{mm} and $T_{m\bar{m}}$; see Figs. 6(a) and 6(b). When N increases, more oscillations are induced by the quantum interference among the JCE-scattered waves but with a decrease in amplitude. Ultimately, T_{mm} and $T_{m\bar{m}}$ approach 0.25 for sufficiently large N, being independent of the SP frequency. For the reflection probabilities in Fig. 6(c), they also approximate 0.25 in outside of the two JCE eigenfrequencies. In one sentence, all transmission and reflection probabilities approximate 0.25 for large N in outside of the two JCE eigenfrequencies. Moreover, the absorption in this region tends to be zero, see Fig. 6(d), also owing to the quantum interference caused by the JCEs. Mathematically speaking, the multiplication of many ζ_n in the transfer matrix M is responsible for it. As a result, the i-OWLs with more JCEs can serve as an ideal SP splitter, i.e., all transmission and reflection probabilities approximate 0.25 with no or marginal loss. The minimum number of the JCEs for the splitter depends slightly on the JCE loss. For $\gamma_a = \gamma_c = 0.001\omega_0$ used in Fig. 6, the maximum deviation from 0.25 for all transmission and reflection probabilities is ~0.014 when $N = 2^4$, which indicates that the present method is valid for designing an ideal SP splitter.

For understanding the extension behavior of N, the spectra are numerically calculated for N up to 2^{10}, though these cases are difficult for experimentalists. The absorption increases for increasing N when ε is between the two JCE eigenfrequencies, except the central point of ω_0. The former is intuitive because each JCE enhances the system loss, while the latter also originates from the quantum interference caused by the JCEs or the multiplication of many ζ_n in M, since the point of ω_0 is the farther point away from the two JCE eigenfrequencies between them. At the point of ω_0, the i-OWLs for very large N (e.g., 2^{10}) also behave like an ideal splitter. The transmission probabilities all tend to be 0.25 between the two JCE eigenfrequencies, and thus the SPs have half a chance to be transmitted and half a chance to be reflected or absorbed. Under the limitation of N the transmission and reflection spectra show weak dependence on the system parameters, such as losses, indicating that the quantum interference caused by the JCEs plays an important role for the SP transport within the i-OWLs. Especially, if the i-OWLs contain a large number of the JCEs, all the transmission and reflection probabilities approximate 0.25, which shows potential for a SP splitter.

B. d-OWLs

The two waveguides in the OWLs could have different group velocities whose influence on the SP transport is focused by the present subsection. Different group velocities commonly result in different SP wave vectors, which is the key difference between the d-OWLs and i-OWLs. Since the transmission and reflection for the d-OWLs with one JCE do not explicitly depend on the wave vectors, see Eq. (23), their spectra are the same as those of the i-OWLs also with one JCE and, therefore, they are not shown here.

However, when the d-OWLs include two JCEs, their transmission and reflection spectra depend on the wave vectors and, accordingly, are different from those of the i-OWLs. Considering that their analytical expressions are too involuted, we only show their numerical results in Fig. 7. Comparing Fig. 7 with Figs. 3(a)–3(c), one can see the spectra differences between the d-OWLs and i-OWLs both with two JCEs. For the d-OWLs, it does not have $T_{11} = T_{22}$ or $R_{11} = R_{22}$, while still holding $T_{21} = T_{12}$ and $R_{21} = R_{12}$. The different group velocities and system reversibility are responsible for them, respectively. The period of T and R with Δx is about $2\lambda_0$ for the d-OWLs, which is different from $0.5\lambda_0$ for the i-OWLs. It can be understood as follows. For the d-OWLs k_1 ($\sim k_0$) and k_2 ($\sim 1.5k_0$) give the periods of λ_0 and $\frac{2}{3}\lambda_0$ for the two waveguides and $2\lambda_0$ is their least common multiple; see Fig. 7. This periodical variation provides a chance for the reflection probabilities up to 0.7 in the d-OWLs, which is larger than 0.25 in the i-OWLs, comparing Figs. 7(b), 7(e) and 7(f) with 3(c). On the other hand, T_{21} and T_{12} can no longer approximate 1, see Fig. 7(c), indicating that the d-OWLs are not suitable for the SP router. These facts indicate that the quantum interference caused by the two JCEs plays an important role in both i-OWLs and d-OWLs structures and thus it is a source for designing optical devices.

Similar to the i-OWLs, the large Δx can also result in many oscillations in the transmission and reflection spectra for the d-OWLs; see Fig. 8. These oscillations, roughly speaking, have a weaker amplitude with respect to those for the i-OWLs in Fig. 4, because different group velocities make the SP transport be out of step in the two waveguides. For the same reason, the quantum interference caused by the two JCEs cannot make T_{21} and T_{12} up to 1, see Fig. 8(c), which is consistent with the case for small Δx; see Fig. 7(c). In

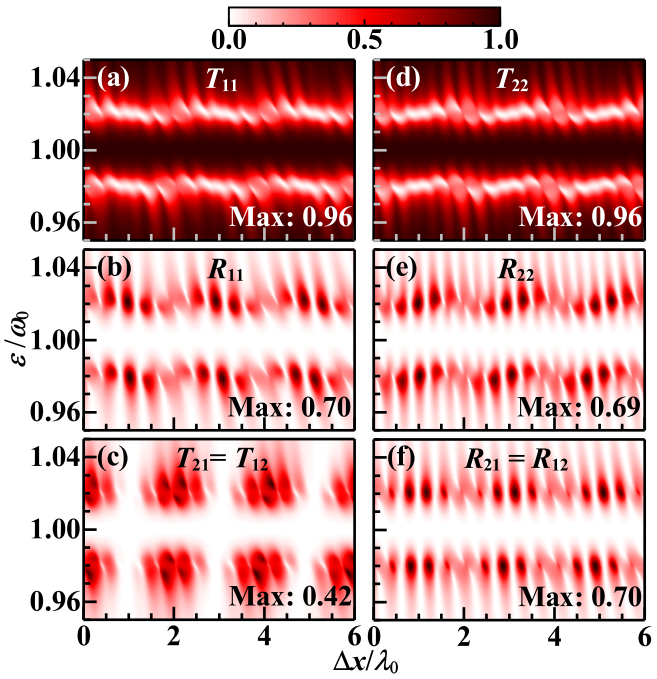

FIG. 7. Contour maps of the transmission and reflection spectra for the d-OWLs with two JCEs ($N = 2$), as functions of the photon energy, ε, and distance between the two JCEs, Δx. Their values are normalized to their maxima denoted by "Max". Parameters: $\omega_c = \omega_a = \omega_0$, $\Omega = 0.02\omega_0$, $J_1 = J_2 = 0.005\omega_0$, $k_1^0 = k_0$, $k_2^0 = 1.5k_0$, $v_1^g = 0.6c$, $v_2^g = 0.9c$, and $\gamma_a = \gamma_c = 0.001\omega_0$.

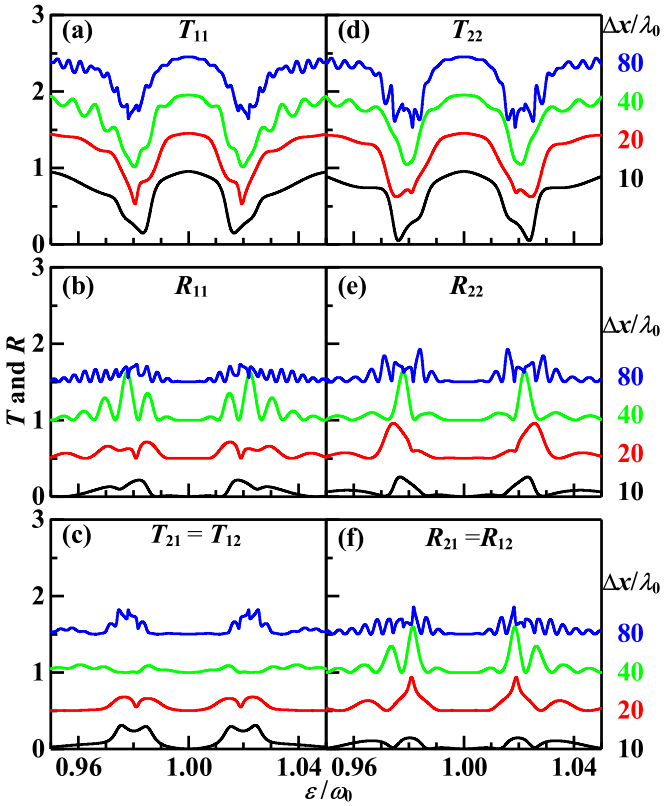

FIG. 8. Transmission and reflection spectra for the d-OWLs with two JCEs ($N = 2$) under four large values of Δx. Lines are offset from the bottom with a step of 0.5. Other parameters are the same as those for Fig. 7.

addition, the value of Δx being an integer multiple of λ_0 is responsible for the bilateral symmetry of all spectra about the axis of $\varepsilon = \omega_0$.

In Fig. 9, we also show the transmission, reflection, and absorption spectra for the d-OWLs with N JCEs. All transmission spectra (i.e., T_{11}, T_{22}, T_{21}, T_{12}) have the same limit of zero for increasing N, see Figs. 9(a), 9(c), and 9(e), indicating that enough JCEs in d-OWLs could fully depress the SP transmission. It is obviously different from that in the i-OWLs where they tend to be the value of 0.25; see Figs. 6(a) and 6(b). This difference can also be attributed to the SP out-of-step transport in the two waveguides in the d-OWLs. On the other hand, the values of all reflection spectra (i.e., R_{11}, R_{22}, R_{21}, R_{12}) for the d-OWLs do not change much but with different shapes. For large N there is a sharp peak near ω_0 for R_{11} [see Fig. 9(b)], while none for R_{22} [see Fig. 9(f)]. In addition, there are two wide reflection bands near the two JCE eigenfrequencies for R_{11}, while just two peaks for R_{22}. The absorption spectra for A_1 and A_2 are also different from each other; see Figs. 9(d) and 9(h). They cannot decrease to zero by increasing N outside of the two JCE eigenfrequencies, which is different from the case for the i-OWLs; see Fig. 6(d). To sum up, enough JCEs in the d-OWLs can fully depress the SP transmission in a very wide wavelength range. This can be achieved when the number of the JCEs is not too large, for example, 2^4 [see Figs. 9(a), 9(c) and 9(e)].

IV. ENTANGLEMENT

Compared with the SWS, the present OWLs have two output channels (see Fig. 1), so that the entanglement between them can be defined for the SP. In this section we first introduce the entanglement definition and then discuss its behavior in the i-OWLs and d-OWLs.

The transmitted SP wave is the superposition of the states from two channels, which can be written as

$$|T\rangle = t_1|1, 0\rangle + t_2|0, 1\rangle. \tag{27}$$

$t_m = t_{m,N}$ denotes the transmission coefficients of the mth channel and $|1, 0\rangle$ ($|0, 1\rangle$) represents the SP state from the port of Out 1 (Out 2). The density matrix of $|T\rangle$ is

$$\hat{\rho} = |T\rangle\langle T| = \begin{pmatrix} |t_1|^2 & t_1 t_2^* \\ t_1^* t_2 & |t_2|^2 \end{pmatrix}, \tag{28}$$

which is expressed under the basis of $\{|1, 0\rangle, |0, 1\rangle\}$. Since $|T\rangle$ is similar to the Bell state, its entanglement can be defined by the von Neumann entropy, i.e.,

$$S = -|t_1|^2 \log_2(|t_1|^2) - |t_2|^2 \log_2(|t_2|^2), \tag{29}$$

which measures the entanglement of the SP states from the two output channels.

Figure 10 shows the entanglement spectra for the i-OWLs and d-OWLs both with one JCE, which have two entropy humps around the two JCE eigenfrequencies. For the i-OWLs, the transmitted SP has the same entropy no matter which

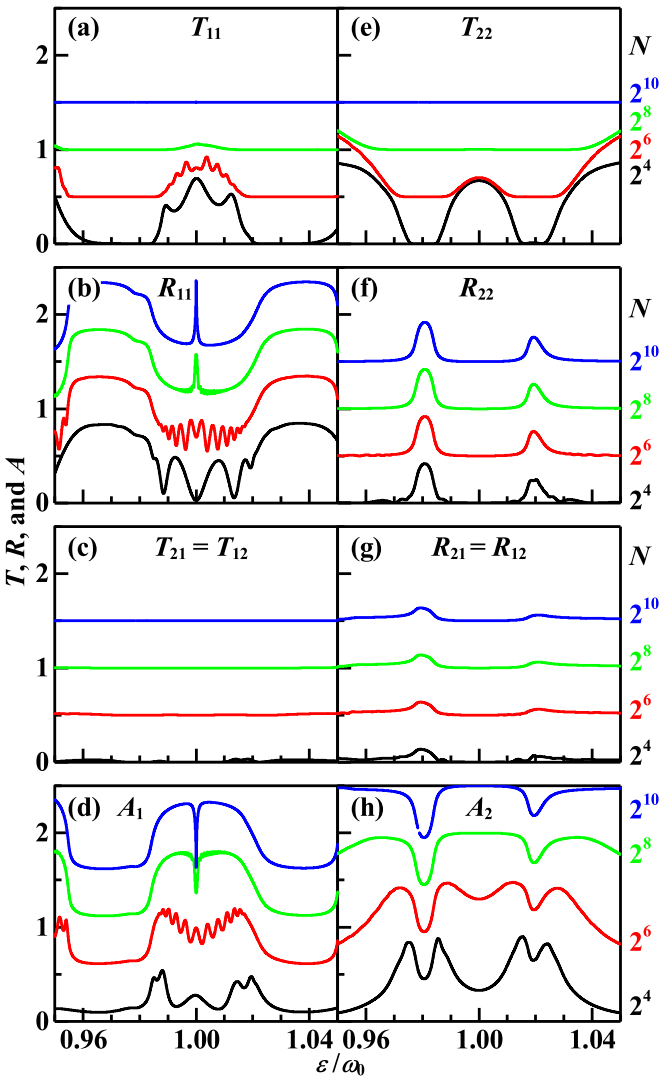

FIG. 9. Transmission, reflection, and absorption spectra for the d-OWLs with N JCEs. All JCEs are uniformly spaced and the nearest-neighbor distance is $\Delta x = 0.5\lambda_0$. Lines are offset from the bottom with a step of 0.5. In calculation, $\gamma_a = \gamma_c = 0.001\omega_0$ and other parameters are the same as those for Fig. 7.

channel it is incident from, while these two entropies are different from each other for the d-OWLs and are higher and lower than that for the i-OWLs, respectively. Interestingly, the entropy given by the dotted green line in Fig. 10 can be larger than 1, which is attributed to that the quantum state in Eq. (27) is not normalized. The reasons for that the equation (27) is not normalized are (a) the dissipation of the cavity and atom are considered and (b) there is photon reflection in the system. These two factors both lead to $|t_1|^2 + |t_2|^2 \leqslant 1$. Under the condition of $|t_1|^2 + |t_2|^2 \leqslant 1$ the entropy can have the largest value of $\frac{2}{e}\log_2 e \approx 1.06$ as $|t_1|^2 = |t_2|^2 = \frac{1}{e}$, a little larger than 1 with respect to the common condition of $|t_1|^2 + |t_2|^2 = 1$. Figure 10 indicates that the different group velocities in the two waveguides can induce a larger entanglement between the SP transmitted states from the two channels.

Figure 11 shows the influence of the quantum interference caused by the two JCEs on the entropies for the i-OWLs and

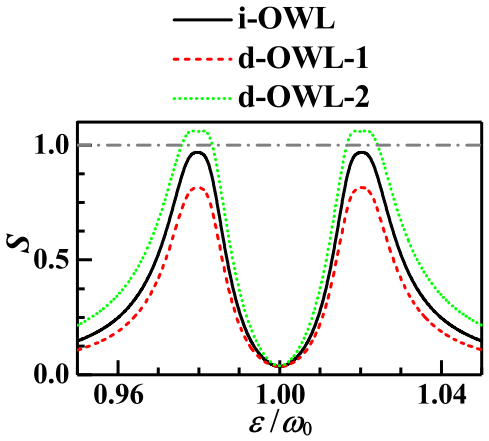

FIG. 10. Entanglement spectra for the i-OWLs and d-OWLs with one JCE ($N = 1$). The number after d-OWL denotes the incident channel of the SP. In calculation, $\gamma_a = \gamma_c = 0.001\omega_0$ and other parameters for the i-OWLs and d-OWLs are the same as those in Figs. 3 and 7, respectively.

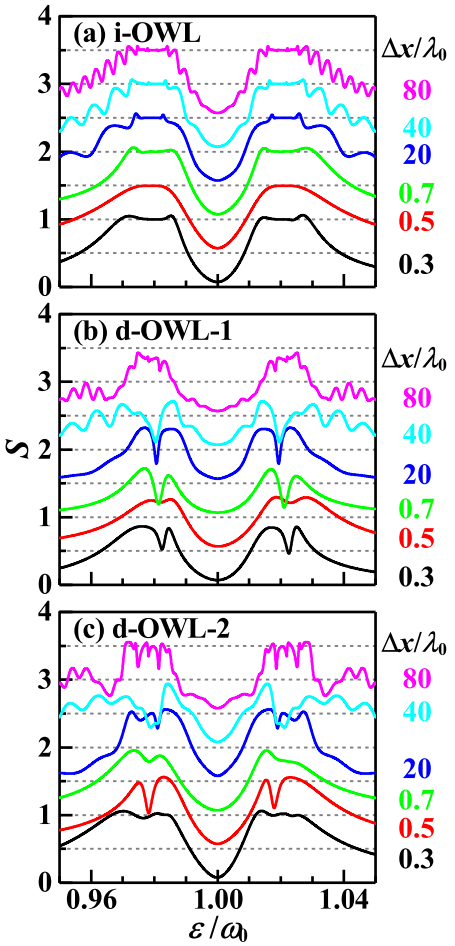

FIG. 11. Entanglement spectra for the (a) i-OWLs and (b), (c) d-OWLs with two JCEs ($N = 2$) under several small and large Δx. In (b) and (c) the SP is incident from the first and second channels, respectively. Lines are offset from the bottom with a step of 0.5. In calculation, $\gamma_a = \gamma_c = 0.001\omega_0$ and other parameters for the i-OWLs and d-OWLs are the same as those in Figs. 3 and 7, respectively.

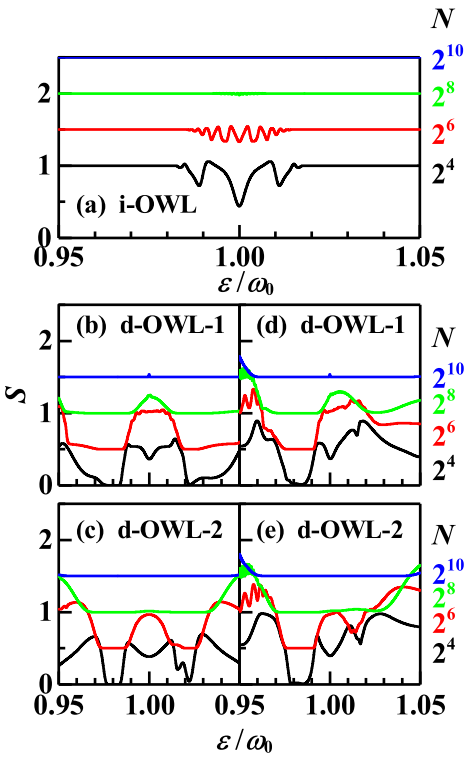

FIG. 12. Entanglement spectra for the (a) i-OWLs and (b)–(e) d-OWLs with N JCEs (N is given on the right side). In (b), (d) and (c), (e) the SP is incident from the first and second channels, respectively. Lines are offset from the bottom with a step of 0.5. In calculation, $\Delta x = 0.5\lambda_0$, $\gamma_a = \gamma_c = 0.001\omega_0$ and other parameters for the i-OWLs and d-OWLs in (b), (c) are the same as those in Figs. 3 and 7, respectively. For (d), (e), $v_1^g = 0.6c$, $v_2^g = 0.7c$, $k_1^0 = k_0$, $k_2^0 = 7k_0/6$, and other parameters are the same as those in Fig. 7.

d-OWLs with two JCEs. Similar to Fig. 10, the entropies for the SP incident from the two channels are the same as each other for the i-OWLs, while being different for the d-OWLs. But they all present more and more oscillations with increasing Δx, owing to the quantum interference caused by the two JCEs; see Fig. 11. Comparing Fig. 11(a) with Fig. 10, the quantum interference widens the two entropy humps for the i-OWLs no matter what the value of Δx is. Since the d-OWLs have different group velocities, their entropy curves are complicated and have a certain randomness; see Figs. 11(b) and 11(c). Roughly speaking, the entropy is larger for the SP incident from the second waveguide than that from the first one. A conclusion can be drawn that the quantum interference caused by the JCEs shows important influence on the entanglement for the two transmitted states, thus providing a way to adjust the entanglement.

The effect of the number of the JCEs (i.e., N) is drawn in Fig. 12. For the i-OWLs the variation of the entropy is consistent with that of T_{11} and T_{21} because of $T_{11} = |t_1|^2$ and $T_{21} = |t_2|^2$. For sufficiently large N, the entropy has a constant value of 1 in almost full wavelength range (where $|t_1|^2 = |t_2|^2 = 0.25$); see Figs. 12(a) and 6(a), 6(b). For finite N this range shrinks and the part near ω_0 is excluded. For example, the entropy approaches 1 only in the outside of the two JCE eigenfrequencies when $N = 2^4$, see the black solid line in Fig. 12(a). Different from the i-OWLs, the entropy in the d-OWLs tends to be zero for large N, because its transmission probabilities of T_{11} and T_{22} tend to be zero; see Figs. 12(b), 12(c) and 9(a), 9(e). As the difference between the two waveguides becomes slight, more JCEs are required for the entropy tending to be zero in the d-OWLs, comparing Figs. 12(d), 12(e) (where $v_1^g/v_2^g = 6/7$) with Figs. 12(b), 12(c) (where $v_1^g/v_2^g = 6/9$), respectively. When N is finite, the region where the entropy has a large value is around the energy of ω_0. For example, the values of the lines with $N = 2^4$ and 2^6 in Figs. 12(b)–12(e) approximate 0.5. In general, the entropy is hard to reach 1 for the d-OWLs, being fully different from that in the i-OWLs. Since the entropy shows very weak dependence on other parameters such as the loss as N is large and approximates a constant value of 1, the i-OWLs can serve as an entanglement generator for the SPs.

V. CONCLUSION

Family properties of the SP transport in the OWLs composed of two 1D waveguides connected by many JCEs were studied by the transfer and scattering matrix theories. When only one JCE is considered, the transmission and reflection spectra for the i-OWLs and d-OWLs are the same as each other, since they do not explicitly depend on the waveguide group velocities. With respect to the structure of one waveguide coupled with one JCE, the influence of the second waveguide in the i-OWLs can be taken as the loss of the cavity. When more than one JCEs are considered, the quantum interference caused by them makes the SP transport properties in the i-OWLs and d-OWLs different. When two JCEs are considered, the quantum interference enables the SP to be able to jump with a 100% chance between two waveguides in the i-OWLs, while it is hard in the d-OWLs. Therefore, the i-OWLs with two JCEs can serve as a SP router. Simultaneously, their transmission and reflection spectra all present more and more oscillation peaks with the increasing distance between two JCEs. The sharpness of these oscillations can be reduced by the dissipations of the JCEs which, therefore, smooth the transmission and reflection spectra. As the number of the JCEs increases to a large value (e.g., 16), the transmission probabilities tend to be 0.25 for the i-OWLs, but zero for the d-OWLs, which shows potential for the i-OWLs with a large number of the JCEs as a SP splitter.

Finally, we use the von Neumann entropy to describe the entanglement between the transmitted states from the two output channels. The entanglements for the SPs incident from the two input channels are the same as each other for the i-OWLs, while are different for the d-OWLs. When OWLs contain only one JCE, the entanglements are always less than 1 for the i-OWLs, but can be larger than 1 for the d-OWLs. If more JCEs are considered, the entanglement spectra become complicated due to the quantum interference among the JCE-scattered waves. Especially when the number of JCEs is sufficiently large (e.g., 16), the entanglements approximate a constant of 1 for the i-OWLs, but of zero for the d-OWLs. This indicates that a large number of JCEs can suppress the influence of other system parameters such as SP frequency and JCE loss and the i-OWLs with a large number of the JCEs can also serve as an entanglement generator for the SPs.

ACKNOWLEDGMENT

This work is supported by the National Natural Science Foundation of China (Grant No. 11304015).

APPENDIX A: DERIVATION FOR $\boldsymbol{M}_n$

To derive $\boldsymbol{M}_n$, one can substitute Eqs. (1) and (5) into (10) and obtain

$$-iv_m^g\frac{\partial}{\partial x}\mathcal{R}_m(x)+\sum_{n=1}^{N}V_{m,n}\delta(x-x_n)\mathcal{C}_n=\bar{\varepsilon}_m\mathcal{R}_m(x), \tag{A1a}$$

$$iv_m^g\frac{\partial}{\partial x}\mathcal{L}_m(x)+\sum_{n=1}^{N}V_{m,n}\delta(x-x_n)\mathcal{C}_n=\bar{\varepsilon}_m\mathcal{L}_m(x), \tag{A1b}$$

$$\sum_{m=1}^{2}V_{m,n}[\mathcal{R}_m(x_n)+\mathcal{L}_m(x_n)]+\Omega_n\mathcal{A}_n=(\varepsilon-\tilde{\omega}_n^c)\mathcal{C}_n, \tag{A1c}$$

$$\Omega_n\mathcal{C}_n=(\varepsilon-\tilde{\omega}_n^a)\mathcal{A}_n, \tag{A1d}$$

where $\bar{\varepsilon}_m=\varepsilon-\omega_0+v_m^gk_m^g$, $\tilde{\omega}_n^a=\tilde{\omega}_n^e-\omega^g$ (ω^g is taken as the energy reference point), and ε is the SP energy. Further substituting Eqs. (6) and (7) into (A1), the transmission and reflection coefficients of $t_{m,n}$ and $r_{m,n}$ are

$$t_{m,n}=t_{m,n-1}-\sum_{m'=1}^{2}\frac{iV_{m,n}V_{m',n}/v_m^g}{(\varepsilon-\tilde{\omega}_n^c)-\frac{\Omega_n^2}{\varepsilon-\tilde{\omega}_n^a}}\times[e^{-i(k_m-k_{m'})x_n}t_{m',n-1}+e^{-i(k_m+k_{m'})x_n}r_{m',n-1}], \tag{A2a}$$

$$r_{m,n}=r_{m,n-1}+\sum_{m'=1}^{2}\frac{iV_{m,n}V_{m',n}/v_m^g}{(\varepsilon-\tilde{\omega}_n^c)-\frac{\Omega_n^2}{\varepsilon-\tilde{\omega}_n^a}}\times[e^{i(k_m+k_{m'})x_n}t_{m',n-1}+e^{i(k_m-k_{m'})x_n}r_{m',n-1}]. \tag{A2b}$$

Then we introduce the transfer matrix of $\boldsymbol{M}_n$

$$\begin{pmatrix}\boldsymbol{t}_n\\ \boldsymbol{r}_n\end{pmatrix}=\boldsymbol{M}_n\begin{pmatrix}\boldsymbol{t}_{n-1}\\ \boldsymbol{r}_{n-1}\end{pmatrix}=\begin{pmatrix}\boldsymbol{M}_n^{tt} & \boldsymbol{M}_n^{tr}\\ \boldsymbol{M}_n^{rt} & \boldsymbol{M}_n^{rr}\end{pmatrix}\begin{pmatrix}\boldsymbol{t}_{n-1}\\ \boldsymbol{r}_{n-1}\end{pmatrix}, \tag{A3}$$

with $\boldsymbol{t}_n=(t_{1,n},t_{2,n})^T$ and $\boldsymbol{r}_n=(r_{1,n},r_{2,n})^T$. Here, $\boldsymbol{M}_n$ is a 4×4 matrix, which can be divided into four 2×2 matrices, i.e., $\boldsymbol{M}_n^{tt}$, $\boldsymbol{M}_n^{tr}$, $\boldsymbol{M}_n^{rt}$, and $\boldsymbol{M}_n^{rr}$. They can be found as

$$\boldsymbol{M}_n^{tt}(m,m')=\frac{1}{\sqrt{v_m^g}}e^{-ik_mx_n}\left[\delta_{mm'}-\frac{i\sqrt{J_{m,n}J_{m'n}}}{\zeta_n}\right]e^{ik_{m'}x_n}\sqrt{v_{m'}^g}, \tag{A4a}$$

$$\boldsymbol{M}_n^{tr}(m,m')=\frac{1}{\sqrt{v_m^g}}e^{-ik_mx_n}\left[-\frac{i\sqrt{J_{m,n}J_{m'n}}}{\zeta_n}\right]e^{-ik_{m'}x_n}\sqrt{v_{m'}^g}, \tag{A4b}$$

$$\boldsymbol{M}_n^{rt}(m,m')=\frac{1}{\sqrt{v_m^g}}e^{ik_mx_n}\left[\frac{i\sqrt{J_{m,n}J_{m'n}}}{\zeta_n}\right]e^{ik_{m'}x_n}\sqrt{v_{m'}^g}, \tag{A4c}$$

$$\boldsymbol{M}_n^{rr}(m,m')=\frac{1}{\sqrt{v_m^g}}e^{ik_mx_n}\left[\delta_{mm'}+\frac{i\sqrt{J_{m,n}J_{m'n}}}{\zeta_n}\right]e^{-ik_{m'}x_n}\sqrt{v_{m'}^g}, \tag{A4d}$$

where $J_{m,n}=\frac{V_{m,n}^2}{v_m^g}$ and $\zeta_n=\varepsilon-\tilde{\omega}_n^c-\frac{\Omega_n^2}{\varepsilon-\tilde{\omega}_n^a}$.

Using the matrices $\boldsymbol{I}$, $\boldsymbol{Y}_n$, $\boldsymbol{G}$, and $\boldsymbol{Q}_n$ defined in Eqs. (12)–(14), we can write the matrix of $\boldsymbol{M}_n$ in a compact form, i.e.,

$$\boldsymbol{M}_n=\boldsymbol{G}^{-1}\boldsymbol{Q}_n^*\begin{pmatrix}\boldsymbol{I}-i\boldsymbol{Y}_n & -i\boldsymbol{Y}_n\\ i\boldsymbol{Y}_n & \boldsymbol{I}+i\boldsymbol{Y}_n\end{pmatrix}\boldsymbol{Q}_n\boldsymbol{G}, \tag{A5}$$

which is Eq. (11).

APPENDIX B: DERIVATION FOR EQ. (21)

In the present Appendix, we show the derivation of Eq. (21). We denote the inverse matrix of $\boldsymbol{M}_n$ as $\boldsymbol{W}_n$ and divide it into four 2×2 matrices, i.e.,

$$\boldsymbol{W}_n=\boldsymbol{M}_n^{-1}=\begin{pmatrix}\boldsymbol{W}_n^{tt} & \boldsymbol{W}_n^{tr}\\ \boldsymbol{W}_n^{rt} & \boldsymbol{W}_n^{rr}\end{pmatrix}. \tag{B1}$$

Subsequently,

$$\begin{pmatrix}\boldsymbol{t}_{n-1}\\ \boldsymbol{r}_{n-1}\end{pmatrix}=\begin{pmatrix}\boldsymbol{W}_n^{tt} & \boldsymbol{W}_n^{tr}\\ \boldsymbol{W}_n^{rt} & \boldsymbol{W}_n^{rr}\end{pmatrix}\begin{pmatrix}\boldsymbol{t}_n\\ \boldsymbol{r}_n\end{pmatrix}. \tag{B2}$$

From Eq. (20), one can further get

$$\begin{pmatrix}\boldsymbol{t}_{n-1}\\ \boldsymbol{r}_0\end{pmatrix}=\begin{pmatrix}\boldsymbol{S}_{n-1}^{tt} & \boldsymbol{S}_{n-1}^{tr}\\ \boldsymbol{S}_{n-1}^{rt} & \boldsymbol{S}_{n-1}^{rr}\end{pmatrix}\begin{pmatrix}\boldsymbol{t}_0\\ \boldsymbol{r}_{n-1}\end{pmatrix}. \tag{B3}$$

Using Eq. (B2), one can replace $\boldsymbol{t}_{n-1}$ and $\boldsymbol{r}_{n-1}$ in Eq. (B3) with $\boldsymbol{t}_n$ and $\boldsymbol{r}_n$, and subsequently obtain

$$\boldsymbol{t}_n=\left(\boldsymbol{W}_n^{tt}-\boldsymbol{S}_{n-1}^{tr}\boldsymbol{W}_n^{rt}\right)^{-1}\boldsymbol{S}_{n-1}^{tt}\boldsymbol{t}_0+\left(\boldsymbol{W}_n^{tt}-\boldsymbol{S}_{n-1}^{tr}\boldsymbol{W}_n^{rt}\right)^{-1}\left(\boldsymbol{S}_{n-1}^{tr}\boldsymbol{W}_n^{rr}-\boldsymbol{W}_n^{tr}\right)\boldsymbol{r}_n, \tag{B4a}$$

$$\boldsymbol{r}_0=\boldsymbol{S}_{n-1}^{rt}+\boldsymbol{S}_{n-1}^{rr}\boldsymbol{W}_n^{rt}\left(\boldsymbol{W}_n^{tt}-\boldsymbol{S}_{n-1}^{tr}\boldsymbol{W}_n^{rt}\right)^{-1}\boldsymbol{S}_{n-1}^{tt}\boldsymbol{t}_0+\boldsymbol{S}_{n-1}^{rr}\left[\boldsymbol{W}_n^{rt}\left(\boldsymbol{W}_n^{tt}-\boldsymbol{S}_{n-1}^{tr}\boldsymbol{W}_n^{rt}\right)^{-1}\left(\boldsymbol{S}_{n-1}^{tr}\boldsymbol{W}_n^{rr}-\boldsymbol{W}_n^{tr}\right)+\boldsymbol{W}_n^{rr}\right]\boldsymbol{r}_n. \tag{B4b}$$

Comparing Eq. (B4) with Eq. (20), the connection between $\boldsymbol{S}_n$ and $\boldsymbol{S}_{n-1}$ can be derived as follows:

$$\begin{aligned}\boldsymbol{S}_n^{tt}&=\left(\boldsymbol{W}_n^{tt}-\boldsymbol{S}_{n-1}^{tr}\boldsymbol{W}_n^{rt}\right)^{-1}\boldsymbol{S}_{n-1}^{tt},\\ \boldsymbol{S}_n^{tr}&=\left(\boldsymbol{W}_n^{tt}-\boldsymbol{S}_{n-1}^{tr}\boldsymbol{W}_n^{rt}\right)^{-1}\left(\boldsymbol{S}_{n-1}^{tr}\boldsymbol{W}_n^{rr}-\boldsymbol{W}_n^{tr}\right),\\ \boldsymbol{S}_n^{rt}&=\boldsymbol{S}_{n-1}^{rt}+\boldsymbol{S}_{n-1}^{rr}\boldsymbol{W}_n^{rt}\left(\boldsymbol{W}_n^{tt}-\boldsymbol{S}_{n-1}^{tr}\boldsymbol{W}_n^{rt}\right)^{-1}\boldsymbol{S}_{n-1}^{tt},\\ \boldsymbol{S}_n^{rr}&=\boldsymbol{S}_{n-1}^{rr}\left[\boldsymbol{W}_n^{rt}\left(\boldsymbol{W}_n^{tt}-\boldsymbol{S}_{n-1}^{tr}\boldsymbol{W}_n^{rt}\right)^{-1}\left(\boldsymbol{S}_{n-1}^{tr}\boldsymbol{W}_n^{rr}-\boldsymbol{W}_n^{tr}\right)+\boldsymbol{W}_n^{rr}\right],\end{aligned} \tag{B5}$$

which is just Eq. (21).

[1] M.-T. Cheng, Y.-Y. Song, Y.-Q. Luo, and G.-X. Zhao, Commun. Theor. Phys. **55**, 501 (2011).
[2] W.-B. Yan and H. Fan, Phys. Rev. A **90**, 053807 (2014).
[3] Z. Liao, H. Nha, and M. S. Zubairy, Phys. Rev. A **93**, 033851 (2016).
[4] Q. Hu, B. Zou, and Y. Zhang, Phys. Rev. A **97**, 033847 (2018).
[5] Q. Jiang, Q. Hu, B. Zou, and Y. Zhang, Phys. Rev. A **98**, 023830 (2018).
[6] J.-T. Shen, M. L. Povinelli, S. Sandhu, and S. Fan, Phys. Rev. B **75**, 035320 (2007).
[7] J.-T. Shen and S. Fan, Phys. Rev. A **79**, 023838 (2009).
[8] J. Pan, S. Sandhu, Y. Huo, N. Stuhrmann, M. L. Povinelli, J. S. Harris, M. M. Fejer, and S. Fan, Phys. Rev. B **81**, 041101(R) (2010).
[9] S. Sandhu, M. L. Povinelli, and S. Fan, Appl. Phys. Lett. **96**, 231108 (2010).
[10] H.-T. Tan, W.-M. Zhang, and G.-X. Li, Phys. Rev. A **83**, 062310 (2011).
[11] D. Englund, A. Majumdar, A. Faraon, M. Toishi, N. Stoltz, P. Petroff, and J. Vučković, Phys. Rev. Lett. **104**, 073904 (2010).
[12] M.-T. Cheng and Y.-Y. Song, Opt. Lett. **37**, 978 (2012).
[13] J.-F. Huang, T. Shi, C. P. Sun, and F. Nori, Phys. Rev. A **88**, 013836 (2013).
[14] J. T. Shen and S. Fan, Opt. Lett. **30**, 2001 (2005).
[15] J.-T. Shen and S. Fan, Phys. Rev. Lett. **98**, 153003 (2007).
[16] J.-T. Shen and S. Fan, Phys. Rev. A **76**, 062709 (2007).
[17] L. Zhou, Z. R. Gong, Y.-X. Liu, C. P. Sun, and F. Nori, Phys. Rev. Lett. **101**, 100501 (2008).
[18] X. Zang and C. Jiang, J. Phys. B **43**, 215501 (2010).
[19] J. Lu, L. Zhou, H. C. Fu, and L.-M. Kuang, Phys. Rev. A **81**, 062111 (2010).
[20] A. Gonzalez-Tudela, D. Martin-Cano, E. Moreno, L. Martin-Moreno, C. Tejedor, and F. J. Garcia-Vidal, Phys. Rev. Lett. **106**, 020501 (2011).
[21] J.-T. Shen and S. Fan, Phys. Rev. A **79**, 023837 (2009).
[22] J.-Q. Liao and C. K. Law, Phys. Rev. A **87**, 043809 (2013).
[23] L.-M. Duan and H. J. Kimble, Phys. Rev. Lett. **92**, 127902 (2004).
[24] K. Koshino, S. Ishizaka, and Y. Nakamura, Phys. Rev. A **82**, 010301(R) (2010).
[25] T. Shi, S. Fan, and C. P. Sun, Phys. Rev. A **84**, 063803 (2011).
[26] Z. Ji and S. Gao, Opt. Commun. **285**, 1302 (2012).
[27] J.-Q. Liao and C. K. Law, Phys. Rev. A **82**, 053836 (2010).
[28] R. D. Kekatpure, E. S. Barnard, W. Cai, and M. L. Brongersma, Phys. Rev. Lett. **104**, 243902 (2010).
[29] Y. Huang, C. Min, and G. Veronis, Appl. Phys. Lett. **99**, 143117 (2011).
[30] Z. Han and S. I. Bozhevolnyi, Opt. Express **19**, 3251 (2011).
[31] J. Chen, C. Wang, R. Zhang, and J. Xiao, Opt. Lett. **37**, 5133 (2012).
[32] Y.-F. Xiao, M. Li, Y.-C. Liu, Y. Li, X. Sun, and Q. Gong, Phys. Rev. A **82**, 065804 (2010).
[33] X. Tu, L. Y. Mario, and T. Mei, Opt. Express **18**, 18820 (2010).
[34] H. Lu, X. Liu, D. Mao, and G. Wang, Opt. Lett. **37**, 3780 (2012).
[35] D. O'Shea, C. Junge, J. Volz, and A. Rauschenbeutel, Phys. Rev. Lett. **111**, 193601 (2013).
[36] G. Dong, Y. Zhang, M. A. Kamran, and B. Zou, J. Appl. Phys. **113**, 143105 (2013).
[37] T. Shi and S. Fan, Phys. Rev. A **87**, 063818 (2013).
[38] S. Xu, E. Rephaeli, and S. Fan, Phys. Rev. Lett. **111**, 223602 (2013).
[39] K. Xia, G. Lu, G. Lin, Y. Cheng, Y. Niu, S. Gong, and J. Twamley, Phys. Rev. A **90**, 043802 (2014).
[40] N.-C. Kim, J.-B. Li, Z.-J. Yang, Z.-H. Hao, and Q.-Q. Wang, Appl. Phys. Lett. **97**, 061110 (2010).
[41] M.-T. Cheng, X.-S. Ma, M.-T. Ding, Y.-Q. Luo, and G.-X. Zhao, Phys. Rev. A **85**, 053840 (2012).
[42] Z. Liao, X. Zeng, S.-Y. Zhu, and M. S. Zubairy, Phys. Rev. A **92**, 023806 (2015).
[43] C.-H. Yan and L. F. Wei, Phys. Rev. A **94**, 053816 (2016).
[44] D. E. Chang, A. S. Sørensen, E. A. Demler, and M. D. Lukin, Nat. Phys. **3**, 807 (2007).
[45] L. Neumeier, M. Leib, and M. J. Hartmann, Phys. Rev. Lett. **111**, 063601 (2013).
[46] O. Kyriienko and A. S. Sørensen, Phys. Rev. Lett. **117**, 140503 (2016).
[47] J. Pan, Y. Huo, S. Sandhu, N. Stuhrmann, M. L. Povinelli, J. S. Harris, M. Fejer, and S. Fan, Appl. Phys. Lett. **97**, 101102 (2010).
[48] M. Bradford, K. C. Obi, and J.-T. Shen, Phys. Rev. Lett. **108**, 103902 (2012).
[49] J.-T. Shen and S. Fan, Phys. Rev. Lett. **95**, 213001 (2005).
[50] A. Auffèves-Garnier, C. Simon, J.-M. Gérard, and J.-P. Poizat, Phys. Rev. A **75**, 053823 (2007).
[51] O. Astafiev, A. M. Zagoskin, A. A. Abdumalikov, Y. A. Pashkin, T. Yamamoto, K. Inomata, Y. Nakamura, and J. S. Tsai, Science **327**, 840 (2010).
[52] I.-C. Hoi, A. F. Kockum, T. Palomaki, T. M. Stace, B. Fan, L. Tornberg, S. R. Sathyamoorthy, G. Johansson, P. Delsing, and C. M. Wilson, Phys. Rev. Lett. **111**, 053601 (2013).
[53] M. Bajcsy, S. Hofferberth, V. Balic, T. Peyronel, M. Hafezi, A. S. Zibrov, V. Vuletic, and M. D. Lukin, Phys. Rev. Lett. **102**, 203902 (2009).
[54] T. G. Tiecke, J. D. Thompson, N. P. de Leon, L. R. Liu, V. Vuletić, and M. D. Lukin, Nature (London) **508**, 241 (2014).
[55] A. Goban, C.-L. Hung, J. D. Hood, S.-P. Yu, J. A. Muniz, O. Painter, and H. J. Kimble, Phys. Rev. Lett. **115**, 063601 (2015).
[56] J. Bleuse, J. Claudon, M. Creasey, N. S. Malik, J.-M. Gérard, I. Maksymov, J.-P. Hugonin, and P. Lalanne, Phys. Rev. Lett. **106**, 103601 (2011).
[57] I.-C. Hoi, C. M. Wilson, G. Johansson, T. Palomaki, B. Peropadre, and P. Delsing, Phys. Rev. Lett. **107**, 073601 (2011).
[58] A. Laucht, S. Pütz, T. Günthner, N. Hauke, R. Saive, S. Frédérick, M. Bichler, M.-C. Amann, A. W. Holleitner, M. Kaniber, and J. J. Finley, Phys. Rev. X **2**, 011014 (2012).
[59] M. Arcari, I. Söllner, A. Javadi, S. Lindskov Hansen, S. Mahmoodian, J. Liu, H. Thyrrestrup, E. H. Lee, J. D. Song, S. Stobbe, and P. Lodahl, Phys. Rev. Lett. **113**, 093603 (2014).
[60] B. Dayan, A. S. Parkins, T. Aoki, E. P. Ostby, K. J. Vahala, and H. J. Kimble, Science **319**, 1062 (2008).
[61] A. Reiserer and G. Rempe, Rev. Mod. Phys. **87**, 1379 (2015).
[62] J.-S. Huang, J.-H. Zhang, and L. F. Wei, J. Phys. B **51**, 085501 (2018).
[63] J.-S. Huang, J.-W. Wang, Y. Wang, Y.-L. Li, and Y.-W. Huang, Quantum Inf. Process. **17**, 78 (2018).
[64] L. Zhou, L.-P. Yang, Y. Li, and C. P. Sun, Phys. Rev. Lett. **111**, 103604 (2013).
[65] J. Lu, L. Zhou, L.-M. Kuang, and F. Nori, Phys. Rev. A **89**, 013805 (2014).

[66] W.-B. Yan and H. Fan, Sci. Rep. **4**, 4820 (2014).
[67] X. Li and L. F. Wei, Phys. Rev. A **92**, 063836 (2015).
[68] M.-T. Cheng, X.-S. Ma, J.-Y. Zhang, and B. Wang, Opt. Express **24**, 19988 (2016).
[69] T. Tian and L. Song, Opt. Commun. **402**, 557 (2017).
[70] I. Shomroni, S. Rosenblum, Y. Lovsky, O. Bechler, G. Guendelman, and B. Dayan, Science **345**, 903 (2014).
[71] X. Zang and C. Jiang, J. Phys. B: At., Mol., Opt. Phys. **43**, 065505 (2010).
[72] G. Dong, Y. Zhang, J. F. Donegan, B. Zou, and Y. Song, Plasmonics **9**, 1085 (2014).
[73] Y. Wang, Y. Zhang, Q. Zhang, B. Zou, and U. Schwingenschlogl, Sci. Rep. **6**, 33867 (2016).
[74] X.-Y. Chen, F.-Y. Zhang, and C. Li, J. Opt. Soc. Am. B **33**, 583 (2016).
[75] C. W. Gardiner and M. J. Collett, Phys. Rev. A **31**, 3761 (1985).
[76] H. Wei, Y. Zhu, and S. Krishnaswamy, IEEE Photon. Technol. Lett. **27**, 2142 (2015).
[77] A. Salmanpour, S. Mohammadnejad, and A. Bahrami, Opt. Quantum Electron. **47**, 2249 (2015).
[78] J. Petersen, J. Volz, and A. Rauschenbeutel, Science **346**, 67 (2014).